Cement and Concrete Composites 110 (2020) 103601

Contents lists available at ScienceDirect

Cement and Concrete Composites

journal homepage: http://www.elsevier.com/locate/cemconcomp

Novel acid-based geopolymer synthesized from nanosized tubular halloysite: The role of precalcination temperature and phosphoric acid concentration

Baifa Zhang [a,b], Haozhe Guo [a,b], Peng Yuan [a,b,*], Liangliang Deng [a,b], Xuemin Zhong [a,b], Yun Li [a,b], Qiang Wang [a,b], Dong Liu [a,b]

[a] CAS Key Laboratory of Mineralogy and Metallogeny/Guangdong Provincial Key Laboratory of Mineral Physics and Materials, Guangzhou Institute of Geochemistry, Institutions of Earth Science, Chinese Academy of Sciences, Guangzhou, 510640, China
[b] University of Chinese Academy of Sciences, Beijing, 100049, China

ARTICLE INFO

Keywords:
Halloysite
Acid-activation
Geopolymer
Precalcination
Microstructure

ABSTRACT

Halloysite is a hydrated polymorph of kaolinite but possesses a distinctive nanosized tubular structure and surface reactivity. The microstructure and mechanical performance of geopolymers derived from calcined halloysite *via* acid-activation were investigated in this study. The acid-activation products were characterized using a combination of techniques including X-ray diffraction (XRD), Fourier-transform infrared spectroscopy (FTIR), nuclear magnetic resonance (NMR), scanning electron microscopy (SEM), and transmission electron microscopy (TEM). Acid-activation of halloysite calcined at 450 °C by 6 mol/L and 10 mol/L phosphoric acid solution produced metavariscite crystals. When the phosphoric acid concentration was increased to 14 mol/L, the acid-activation product became more compact due to the formation of geopolymer that were mainly composed of Al–O–P networks. Calcination of halloysite at 750 °C led to an active form of halloysite, which was favored by geopolymerization. Higher phosphoric acid concentration led to the incorporation of more Si and P in the geopolymer matrix with Si–O–P–O–Al networks, and thus greater compressive strength. Halloysites calcined at 1000 °C barely reacted with phosphoric acid, due to the nanocrystalline formation and the decreased Si–OH content in the calcined halloysite, which had low reactivity unfavorable for geopolymerization. These results indicated that the microstructure and mechanical performance of halloysite-based geopolymers are highly dependent on the precalcination temperature of halloysite and the phosphoric acid concentration. Suitable precalcination temperature and high concentration of phosphoric acid facilitate high degree of geopolymerization, which is conducive to the formation of an acid-activated halloysite-based geopolymer with excellent mechanical performance.

1. Introduction

Geopolymers are inorganic polymeric materials composed of polyaluminosilicate chains or networks [1–3]. Owing to their three-dimensional network structure, geopolymers exhibit excellent properties in terms of compressive strength, thermal stability, and dilatability [4–6]. Geopolymers have attracted increasing attention in the last decades and are regarded as alternatives to ordinary Portland cement (OPC) because of their better performance and smaller environmental footprint [7–9]. Hence, geopolymeric materials have been widely applied in nuclear waste immobilization [10], waste water treatment [11], and infrastructure construction [12,13]. Geopolymers are synthesized by mixing aluminosilicates (e.g., clay, fly ash, volcanic ash, etc.) with an activator (e.g., sodium silicate, phosphate, etc.) and was then cured at slightly elevated temperature [14–16].

There are two types of geopolymers, alkali-based and acid-based geopolymers, in term of the types of activator. Alkali-based geopolymers, consisting of cross-linked tetrahedral [AlO_4] and [SiO_4] units with hydrated alkali metal cations, are synthesized by the dissolution of aluminosilicates in an alkaline activator [2,17]. In contrast, acid-based

* Corresponding author. CAS Key Laboratory of Mineralogy and Metallogeny, Guangzhou Institute of Geochemistry, Institutions of Earth Science, Chinese Academy of Sciences, Wushan, Guangzhou, 510640, China.
E-mail address: yuanpeng@gig.ac.cn (P. Yuan).

https://doi.org/10.1016/j.cemconcomp.2020.103601
Received 8 November 2019; Received in revised form 17 March 2020; Accepted 23 March 2020
Available online 2 April 2020
0958-9465/

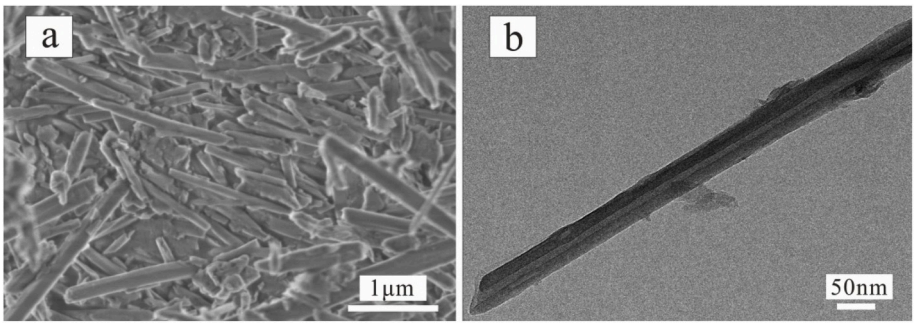

Fig. 1. Morphology of Hal: (a) SEM image, (b) TEM image.

geopolymers are synthesized by the reaction of aluminosilicates with phosphoric acid solution [18]. Having tetrahedral [PO_4] partly in place of [SiO_4], the acid-based geopolymers do not require cations to balance the charge. Therefore, the dielectric loss of acid-based geopolymers is lower than that of alkali-based geopolymers [19]. Additionally, compared to alkali-based geopolymers, acid-based geopolymers have stronger bonding and thus higher compressive strength as well as lower efflorescence and higher thermal stability. These advantages of acid-based geopolymers enable their broad application prospects [20–22].

The microstructures and performance of acid-based geopolymers are influenced by the physicochemical properties of the precursors and activator, such as particle size [23], curing temperatures [24], phosphoric acid concentration [25], and aluminosilicate type [26–28]. Kaolinite ($Al_2(OH)_4Si_2O_5$) is a 1:1 dioctahedral clay mineral with tetrahedral silica sheets and octahedral alumina sheets, which can be transformed into amorphous metakaolinite when heated at 600°C-900 °C [29,30]. Owing to its high reactivity and simple chemical composition, calcined kaolinite is the most commonly used raw materials for the preparation of acid-based geopolymers [24,25].

Halloysite ($Al_2(OH)_4Si_2O_5\bullet 2H_2O$) is a hydrated polymorph of kaolinite, which has an additional water monolayer between the 1:1 aluminosilicate layers that differs with kaolinite [31]. Like kaolinite, halloysite is an inexpensive natural materials because it has huge reserve in nature, although the reported reserve of halloysite is smaller than that of kaolinite [32]. More importantly, as a naturally occurring nanomaterial, halloysite possesses a nanosized tubular structure resulting from the mismatch between its oxygen-sharing tetrahedral and octahedral sheets, and has higher specific surface area than plate-like kaolinite due to its nanosize [33–35]. Furthermore, halloysite is normally poorly ordered, less chemically stable and thereby more reactive than kaolinite [36,37]. The abovementioned features endow halloysite potential advantages over kaolinite in geopolymer preparation and this point has been indicated by a few previous studies [38–40]. For example, Tchakouté et al. [39] compared the mechanical properties of alkali-activated kaolinite-based and halloysite-based geopolymers and concluded that halloysite-based geopolymer showed higher mechanical strength. Kaze et al. [41] prepared an alkali-based geopolymer with a maximum compressive strength of 27.5 MPa from halloysite-rich clay calcined at 600 °C. This result suggests that using halloysite as a raw material for geopolymer preparation may reduce energy consumption. According to Zhang et al. [40] calcined halloysite exhibited higher geopolymerization reactivity than calcined kaolinite, indicated by higher dissolution rate of Si and Al, faster geopolymerization, and faster compressive strength development.

To date, halloysite-based geopolymers formed *via* acid-activation has not been reported. Despite that, a few previous studies focusing on the dissolution of halloysites have indicated that the performance of halloysite under acid-activation and alkali-activation is quite different [36,42], implying that acid-activated and alkali-activated halloysite-based geopolymers may have different formation mechanisms. For example, during acid dissolution of halloysite, silica nanoparticles form in strong acid solution, because silica is less soluble than alumina at low pH; however, in strong alkaline solution, flaky particles comprising $Al(OH)_3$ layers form, because alumina is less soluble than silica at high pH [42]. In addition, hydroxyl groups are formed on the outer surfaces of the nanotubes of halloysite, when halloysite is calcined at 600°C-900 °C [43], which may further complicate the dissolution of calcined halloysite and give rise to the mechanistic differences between alkali-based and acid-based geopolymerization. Therefore, acid-activated halloysite-based geopolymerization is a poorly understood domain of geopolymerization and thus warrants more in-depth studies, which is of significance not only for understanding the related formation mechanisms, but also for the development of novel geopolymeric materials.

In this work, the feasibility of using nanosized tubular halloysite for the synthesis of acid-based geopolymers was evaluated for the first time. The effects of the precalcination temperature of halloysite and concentration of phosphoric acid on the microstructures and mechanical performance of the resultant geopolymer were investigated. A combination of characterization methods, such as X-ray diffraction (XRD), Fourier-transform infrared (FTIR) spectroscopy, and nuclear magnetic resonance (NMR), was used to detect the chemical structure of different halloysite-based geopolymers. The microstructural features and composition of the halloysite-based geopolymers were revealed by scanning electron microscopy (SEM) and transmission electron microscopy (TEM). The determining factors of the formation mechanisms and the structure of acid-activated halloysite-based geopolymers were discussed on the basis of the abovementioned characterizations.

2. Experiment

2.1. Materials

Halloysite (Hal) from the USA was provided by I-Minerals Inc. The chemical composition of Hal measured by X-ray fluorescence is presented as follows: Al_2O_3 (37.80%), SiO_2 (46.00%), Fe_2O_3 (0.72%), K_2O (0.30%), MgO (0.13%), CaO (0.07%), Ti_2O (0.07%), and loss on ignition (14.90%). The specific surface area of Hal was 28.29 m^2/g. The SEM and TEM images (Fig. 1) show that the nanosized Hal particles have tubular morphology and the nanotubes are hollow, indicated by the transparent central areas of the tubes (Fig. 1b). The Hal powder was calcined in a muffle furnace at 450 °C, 750 °C, and 1000 °C in air for 2 h (heating/cooling rate 5 °C/min). The obtained calcined halloysites are labeled as Hal_T, where T represents precalcination temperature. For example, $Hal_{450°C}$ is the product obtained after heating Hal at 450 °C for 2 h. The SEM images of Hal_T are shown in Fig. S1 (Supplementary Information). There was no distinctive change in morphology after being thermally treated at the temperature of 450 °C and 750 °C (Figs. S1a and S1b). Moreover, the halloysite kept its tubular morphology although the tube length became shorter and tended to aggregate when calcined at 1000 °C (Figs. S1c and S1d).

Different concentrations (6 mol/L, 10 mol/L, and 14 mol/L) of

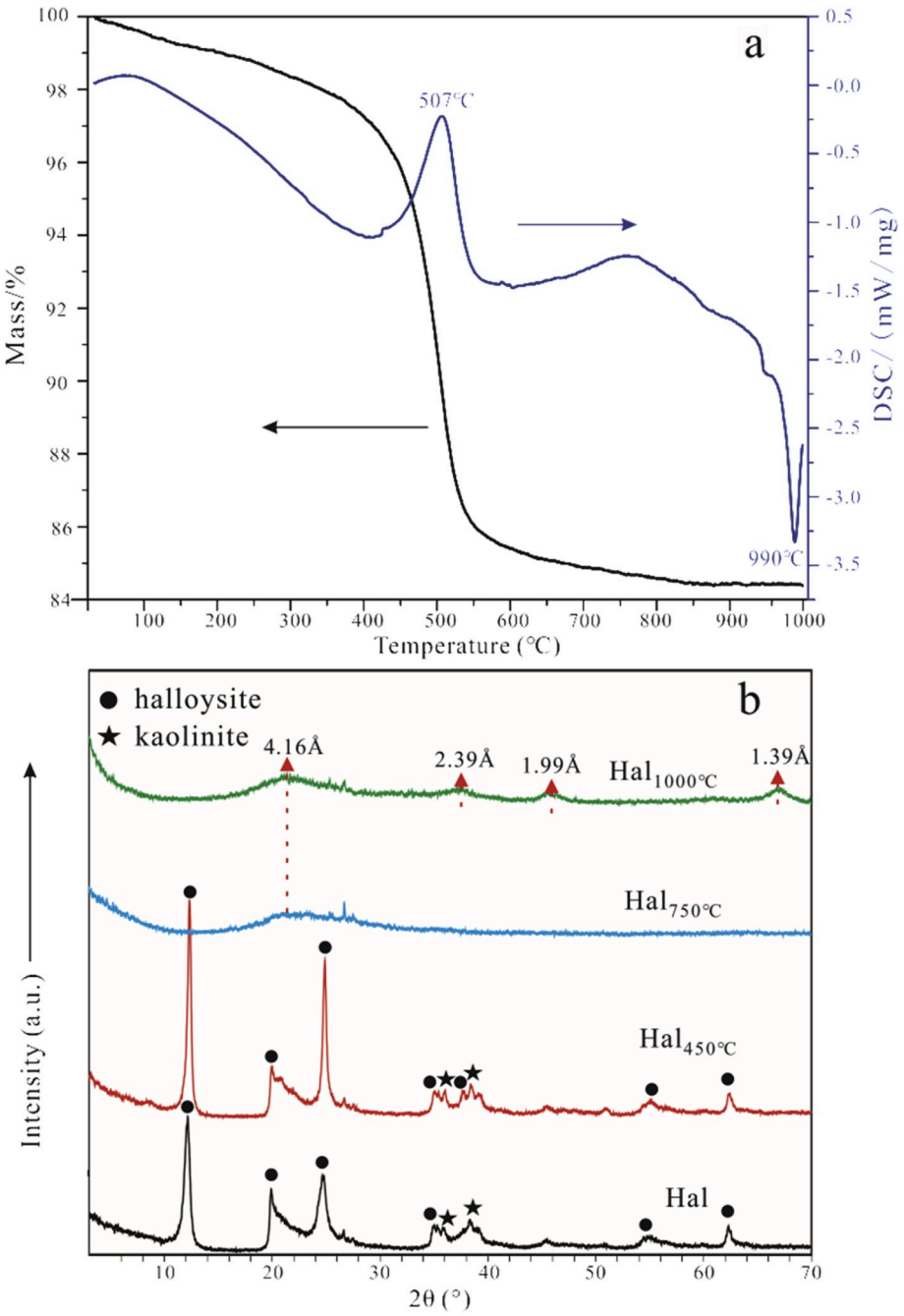

Fig. 2. (a) TG and DSC curves of Hal; (b) XRD patterns of Hal and its heating products.

phosphoric acid solution were prepared by dilution of commercial orthophosphoric acid (H_3PO_4, 85 wt% in H_2O) in ultrapure water. Solutions were stored for 24 h prior to use.

2.2. Preparation of acid-activated Hal_T

To prepare the halloysite-based geopolymers, Hal_T was mixed with certain known concentrations of phosphoric acid solution at a constant liquid/solid ratio of 1.3/1.0. The resulting slurry was cast in 20 × 20 × 12 mm plastic molds and the molded specimens were first cured at 50 °C for 48 h and then were demolded followed by further curing at 80 °C for 48 h. The demolded samples were sealed in the plastic bags and then cured at ambient temperature. The obtained products were labeled as Hal_T-X, where X represents the concentration of phosphoric acid solution.

2.3. Characterization methods

Acid-leaching tests were conducted on calcined halloysite. Thus, 1 g of Hal_T was mixed with 20 mL of 6 mol/L, 10 mol/L, or 14 mol/L phosphoric acid solution, respectively, in a shaker at 25 ± 2 °C for 24 h. The resulting mixture was then centrifuged, and the supernatant was passed through a filter to afford1 mL of clear solution. This solution was diluted to 25 mL with ultrapure water, and the concentration of Si and Al in the diluted solution was then determined by using an iCAP 7000 Series inductively coupled plasma optical emission spectrometer (Thermo Scientific, USA).

Thermogravimetric (TG) and differential scanning calorimetry (DSC) curves were collected by Netzsch STA 409 PC instrument (Selb, Germany). 10 mg of halloysite was put in a corundum crucible and then heated from 30 to 1000 °C.

Acid-activation products cured for periods of 7 d and 28 d were subject to unconfined compression tests on a YAW-300D compression testing machine (LiXian, Zhejiang).

XRD analysis was performed at 40 kV and 40 mA on a Bruker D8 Advance diffractometer (Mannheim, Germany) using CuKα radiation with a scanning step of 3° min^{-1}.

FTIR spectra were recorded on a Bruker Vertex 70 spectrometer (Karlsruhe, Germany). For this, 0.8 mg of crushed sample and 80 mg of KBr were mixed and finely pulverized, and the resulting homogenous powder was pressed into a disk, which was analyzed.

The solid-state ^{29}Si cross-polarization magic-angle-spinning (CP/MAS) NMR spectra, ^{27}Al and ^{31}P MAS NMR spectra were recorded on a BRUKER AVANCE III 600 spectrometer. For ^{29}Si CP/MAS NMR spectra were recorded using a 6 ms contact time, a 2 s recycle delay, and a 10 kHz spinning rate. The chemical shifts of ^{29}Si was given in ppm referenced to 1 mol/L tetramethylsilane. For ^{27}Al MAS NMR spectra were recorded using a small-flip angle technique with a 0.5 μs pulse length, a 1 s recycle delay, and a 14 kHz spinning rate. The chemical shifts of ^{27}Al was given in ppm referenced to 1 mol/L $Al(NO_3)_3$.^{31}P MAS NMR was performed at a resonance frequency of 242.9 MHz using a 4 mm HX double-resonance MAS probe at a 12 kHz spinning rate. Single-pulse ^{31}P MAS NMR experiments with ^{1}H decoupling were performed with a 90° pulse width of 4.9 μs, a 180 s recycle delay, and a ^{1}H decoupling strength of 80 kHz with 160 scans. The chemical shift of ^{31}P was externally referenced to 85% H_3PO_4.

SU8010 field-emission scanning electron microscope (Hitachi, Japan) was used to collect the SEM images and EDX spectroscopy, where the accelerating voltage was set as 15 kV. The as-fractured samples were anchored on the surface of the conducting tape within coated a platinum layer before test.

The TEM images and EDX spectroscopy data were collected on an FEI Talos F200S field-emission TEM at a 200 kV accelerating voltage. The powdered samples were ultrasonically dispersed in ethanol for 10 min and two droplets of the resulting dispersion were dropped onto a carbon-coated copper grid.

3. Results

3.1. Changes in structure and reactivity of Hal under heating

3.1.1. Changes in structure of Hal under heating

Fig. 2a shows the TG and DSC results of Hal. A mass loss was observed in the temperature between 30 °C and 200 °C ascribed to the loss of adsorbed water and interlayer water. Another major weight loss occurred at the temperature range 450°C–550 °C, which was associated with the dehydroxylation of halloysite [44]. In the DSC curve, a narrow exothermic peak at approximately 990 °C was shown. Based on the ^{29}Si and ^{27}Al MAS NMR results, Smith et al. [45] had proposed that this exothermic event during the calcination of halloysite should be attributed the formation of nanosized γ-Al_2O_3. This argument was supported by Yuan et al. [46], who identified the formation of nanosized γ-Al_2O_3 by using high-resolution TEM. Therefore, the precalcination temperatures (450 °C, 750 °C, and 1000 °C) adopted by the present study represented three different stages, dehydration, dihydroxylation, and phase transformation of halloysite under heating, respectively.

Fig. 2b shows the XRD patterns of Hal and Hal_T. The strong reflection at 12.2° (2θ, with a d_{001} of 7.25 Å) in Hal was indexed to halloysite. It can be seen that the diffractions of $Hal_{450°C}$ differed little from those of Hal, indicating that heating at 450 °C caused no structural change in Hal. The characteristic peaks of halloysite were absent from the XRD pattern of $Hal_{750°C}$, and a new broad reflection centered at approximately 21.1° (2θ) (with *d* spacing of 4.16 Å at the central point), which should be attributed to the amorphous silica, indicating the disordering of the structure of Hal due to dehydroxylation [46]. This result indicated that the crystal structure of Hal had been largely destroyed and that the mineral had started to be transformed into a low ordered form [47].

Table 1
Concentration of Al and Si leached from Hal_T in phosphoric acid solutions for 24h.

Precalcination temperature	6 mol/L H_3PO_4		10 mol/L H_3PO_4		14 mol/L H_3PO_4	
	Al (ppm)	Si (ppm)	Al (ppm)	Si (ppm)	Al (ppm)	Si (ppm)
450°C ($Hal_{450°C}$)	458.33	29.50	380.53	8.45	529.76	5.13
750°C ($Hal_{750°C}$)	962.40	20.85	496.61	7.02	816.00	6.60
1000°C ($Hal_{1000°C}$)	66.63	20.48	71.11	7.26	56.93	5.63

When the calcination temperature increased to 1000 °C, new reflections corresponding to *d* values of 2.39 Å, 1.98 Å, and 1.39 Å appeared, which indicated the formation of new phase. As aforementioned, these reflections should be assigned to nanocrystalline γ-Al_2O_3, which was evidenced by a combination of characterizations such as NMR, FTIR and TEM results in previous studies [43,45,46].

3.1.2. Dissolution behavior of Hal_T in phosphoric acid solution

The concentrations of dissolved Si and Al, leached from Hal_T in different concentrations of phosphoric acid solution are summarized in Table 1. It can be seen that the Al concentration in the leached solution was affected by the precalcination temperature of Hal and the concentration of the phosphoric acid.

Compared to $Hal_{450°C}$, $Hal_{750°C}$ showed higher concentration of the leached Al, whereas $Hal_{1000°C}$ exhibited substantially declined concentration of the leached Al (Table 1). This is due to that the structure of $Hal_{750°C}$ was more disordered than $Hal_{450°C}$ and its reactivity was higher accordingly. However, as mentioned above, the formation of nanocrystalline γ-Al_2O_3 in $Hal_{1000°C}$ might result in the reduced dissolution in phosphoric acid. However, for $Hal_{450°C}$ and $Hal_{750°C}$, the elevated concentrations of phosphoric acid solution did not result in a stronger leaching because the concentration of leached Al in 10 mol/L H_3PO_4 were lower than those in 6 mol/L and 14 mol/L H_3PO_4 (Table 1). This result suggests that there existed opposite effects on the dissolution of halloysite in elevated concentration of phosphoric acid solution [48], i.e., dissolution-inhibiting and dissolution-enhancing effects, which resulted in the fluctuation of the concentration of Al in leached solutions. Specifically, higher phosphoric acid concentration not only increased the amount of proton (H^+), but increased the amount of Si-precipitation during dissolution of halloysite. According to Carmen et al. [49], this Si-precipitation (i.e., polymerized silica) could be deposited on the undestroyed aluminosilicate fractions and inhibited it further attack by H^+. Therefore, when the phosphoric acid concentration increased from 6 mol/L to 10 mol/L, more H^+ attacked the structural OH groups of $Hal_{450°C}$ and $Hal_{750°C}$, however, more formed Si-precipitation coated the halloysite and prevented the structural OH groups from further attacking at the meantime [48–50], which resulted in the decreased of leached Al. When the concentration of phosphoric acid increased from 10 mol/L to 14 mol/L, the much more H^+ could penetrate the decomposed halloysite and attacked the OH groups, leading to the increased of dissolved Al. Collectively, owing to different dominant of these opposite effects, the concentration of dissolved Al fluctuated as the concentration of phosphoric acid increased.

Table 1 showed that the concentration of Si in the leached solution was much lower than that of Al and the data in Table 1 suggest that precalcination had little effect on the dissolution of Si. This might be attributed to the similar solubility of silica in high concentrated phosphoric acid solution. Notably, higher phosphoric acid concentration tended to inhibit the dissolution of Si from Hal_T: the leached Si concentration continually decreased as the acid concentration increased. This was due to the more precipitation for Si in higher concentration of acidic solutions [50]. These results illustrated that the dissolution of Hal_T in acid solution has a complex dependence on the reaction conditions, which means that the acid-activation of halloysite is complex.

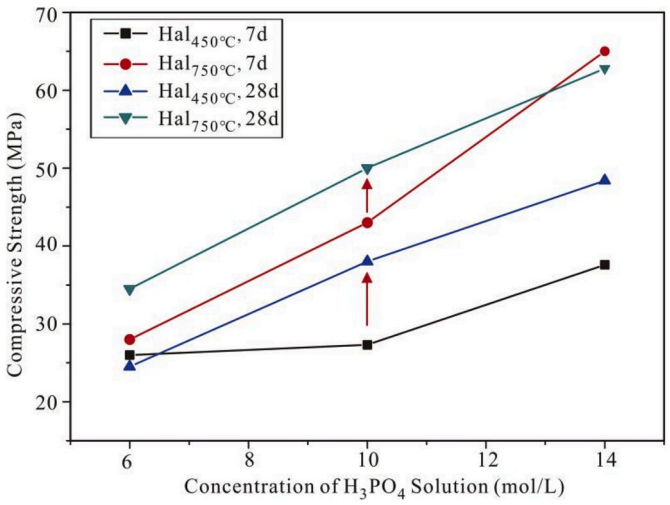

Fig. 3. Compressive strength of acid-activated Hal_T.

3.2. Compressive strength-development of acid-activated Hal_T

Fig. 3 plots the compressive strength of the acid-activation products cured for 7 d and 28 d as a function of phosphoric acid concentration. The acid-activation products prepared from $Hal_{1000°C}$ failed to set and harden under the curing condition adopted in this study, so these products had no compressive strength.

It can be seen that higher acid concentration led to higher compressive strength of the as-obtained products. When the concentration increased from 6 to 14 mol/L, the 7 d compressive strength increased from 26 MPa to 38 MPa for $Hal_{450°C}$-X, while it increased from 28 MPa to 65 MPa for $Hal_{750°C}$-X.

Curing for 28 d improved the compressive strength of $Hal_{450°C}$-10 M, $Hal_{450°C}$-14 M, $Hal_{750°C}$-6M, and $Hal_{750°C}$-10 M, which increased to 38 MPa, 48 MPa, 35 MPa, and 50 MPa, respectively. However, the compressive strength of $Hal_{450°C}$-6M and $Hal_{750°C}$-14 M slightly declined to 25 MPa and 63 MPa at 28 d. In practice, compressive strength development can be affected by many factors, such as curing temperature [24], water content [51], pore distribution [20], and others, which warrants further research.

3.3. Structure of acid-activated Hal_T

3.3.1. XRD results

The XRD pattern of $Hal_{450°C}$-6M illustrated in Fig. 4 contained many reflections that could be indexed to metavariscite ($AlPO_4$•$2H_2O$), a hydrated form of aluminum phosphate, with a d_{002} of 4.21 Å. When the acid concentration increased to 10 mol/L, the reflections attributed to metavariscite increased in intensity and became sharper, indicating that there had been an increase in the metavariscite content. Notably, a major broad reflection centered at 26°(2θ) (with d spacing of 3.40 Å) appeared when the concentration increased to 14 mol/L, which was due to formation of geopolymer [28,52]. The XRD patterns for all $Hal_{750°C}$-X samples were similar to each other. The broad reflection at 4.16 Å for $Hal_{750°C}$ (Fig. 2) shifted to 3.40 Å after acid-activation, confirming that the network had reorganized to form amorphous geopolymer [23]. The XRD patterns showed that some γ-Al_2O_3 remained in $Hal_{1000°C}$ after the

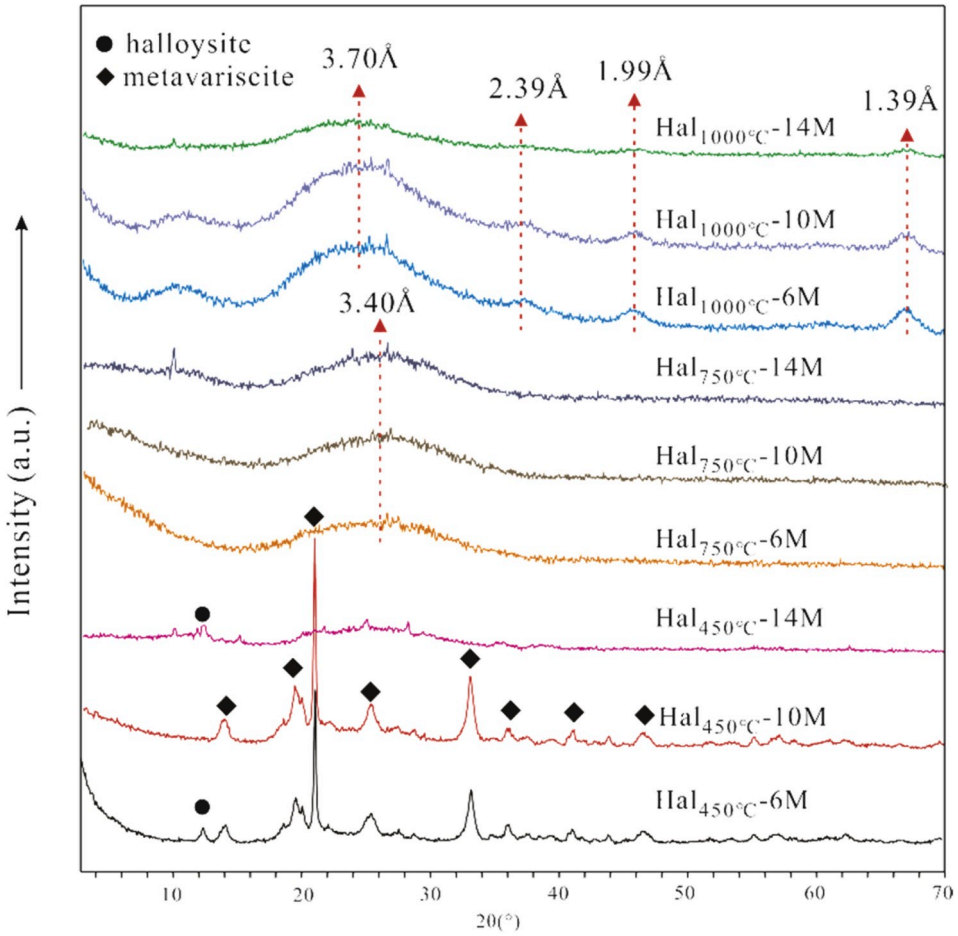

Fig. 4. XRD patterns of acid-activated Hal_T.

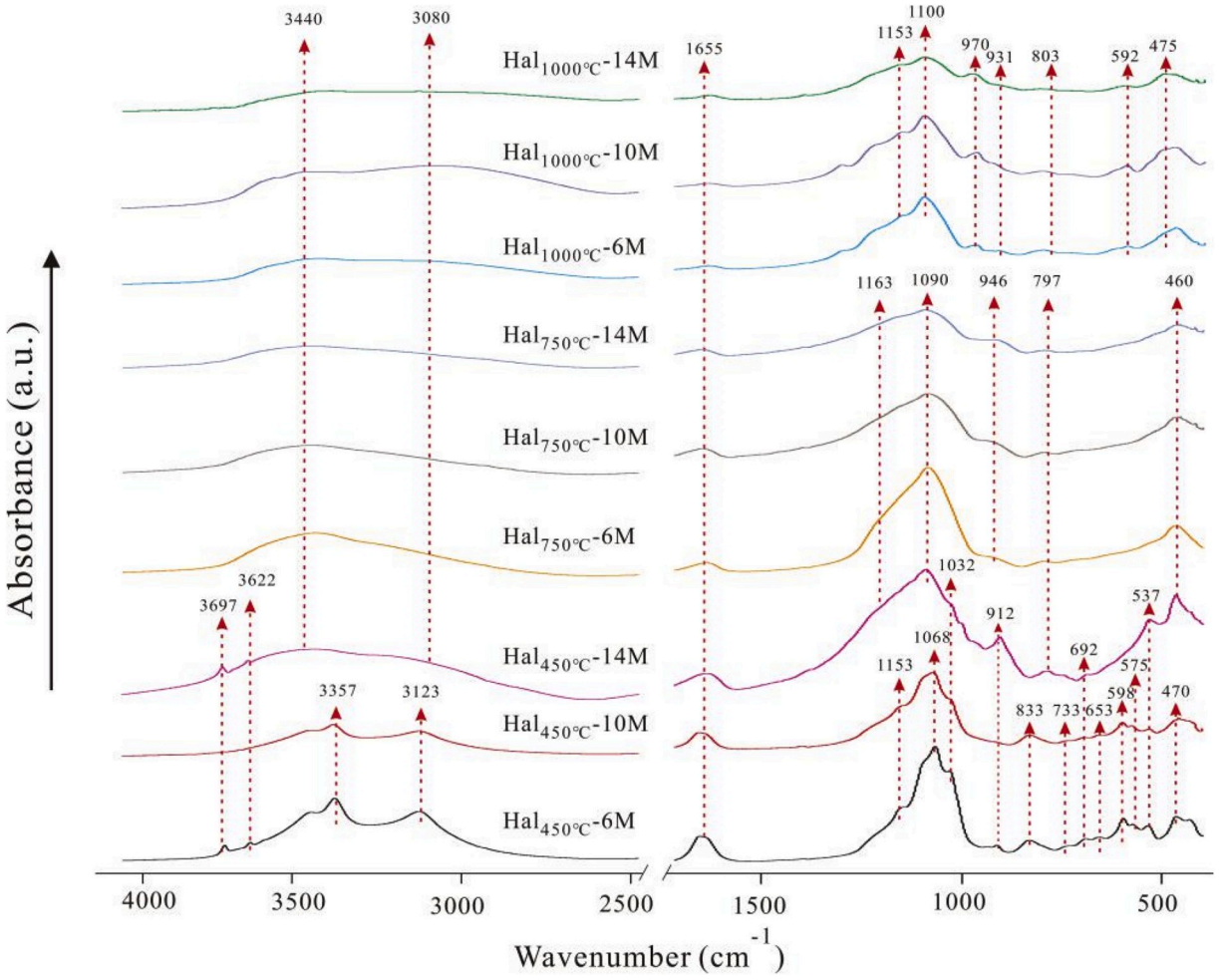

Fig. 5. FTIR patterns of acid-activated Hal_T.

acid-activation; this implied that not all of the Al took part in the geopolymerization, which was in agreement with the results of the leaching test (Table 1).

3.3.2. FTIR results

The FTIR spectra of the acid-activation products are shown in Fig. 5. In the FTIR spectrum of $Hal_{450°C}$-6M, the bands at 3697 cm^{-1}, 3622 cm^{-1}, 1032 cm^{-1}, 692 cm^{-1}, 537 cm^{-1}, and 470 cm^{-1} indicated the presence of unreacted $Hal_{450°C}$ in the product [33,46,53]. Two broad bands at 3375 cm^{-1} and 3123 cm^{-1} were attributed to O–H stretching vibrations of crystallization water from metavariscite, while the band at 833 cm^{-1} was attributed to O–H bending vibration of Si–OH [54]. The shoulder band at 1153 cm^{-1} was tentatively attributed to the amorphous SiO_2 [42]. Generally, P-bond vibrations can be detected at wavenumbers less than 1400 cm^{-1} [55]. Accordingly, the main band at 1068 cm^{-1} was attributed to P–O stretching asymmetric vibrations of [PO_4], while the bands at 598 cm^{-1} and 575 cm^{-1} were assigned to O–P–O deformational bending vibrations [55,56]. An Al–O–P symmetric stretching vibration (733 cm^{-1}) and bending vibration (653 cm^{-1}) were also observable [57]. All these bands were typical for metavariscite. The FTIR spectrum of $Hal_{450°C}$-10 M was like that of $Hal_{450°C}$-6M, indicating that there was little structural difference at the molecular scale between these two products. However, the characteristic peaks of $Hal_{450°C}$-14 M were broader, consistent with the formation of highly amorphous products [43].

It can be seen that the FTIR spectra of acid-activated $Hal_{750°C}$ are almost identical, regardless of acid concentration. The absorptions at ~3440 cm^{-1} and ~1659 cm^{-1} were attributed to O–H stretching and bending vibrations of physically adsorbed water, respectively [58]. The main band at approximately 1090 cm^{-1} was tentatively ascribed to the overlapping P–O and Si–O vibrations [55,59], or was ascribed to P–O–Si vibration [25,60]. It is in fact difficult to completely distinguish the vibrations of [SiO_4] and [PO_4] in phosphosilicate materials, as the bands associated with these two vibrations appear in practically the same range of the FTIR spectrum [55]. The new band at 797 cm^{-1} was related to Si–O–Si stretching vibration [58,60], while that at 460 cm^{-1} was assigned to Si–O–Si in-plane bending vibration [46]. In addition, the shoulder bands at 1169 cm^{-1} and 946 cm^{-1} corresponded to P–O stretching vibration in the structure of the acid-based geopolymer [25,58].

In contrast, $Hal_{1000°C}$-X showed additional characteristic peaks of unreacted H_3PO_4 and $Hal_{1000°C}$, such as the bands at 1153 cm^{-1} (P═O asymmetric stretching vibration from H_3PO_4), 970 cm^{-1} (P–O–P asymmetric stretching vibration from H_3PO_4), 803 cm^{-1} (Al–O vibration of γ-Al_2O_3 from $Hal_{1000°C}$), and 470 cm^{-1} (Si–O–Si vibration from $Hal_{1000°C}$) [25,37]. The main band at ~1100 cm^{-1} was associated with the O–P–O vibration corresponded to [PO_4], while the peaks at ~931 cm^{-1} and ~593 cm^{-1} were assigned to P–O stretching vibration and P═O stretching vibration of [PO_4], respectively [55,59].

3.3.3. NMR results

The ^{27}Al, ^{29}Si, and ^{31}P MAS NMR spectra of Hal_T and their acid-activation products are presented in Fig. 6. The ^{27}Al spectrum for $Hal_{450°C}$ (Fig. 6a) showed a single resonance at 7 ppm, which was ascribed to Al^{VI}. However, the spectrum of Hal calcined at 750 °C showed three broad resonances centered at 7 ppm, 32 ppm, and 58 ppm

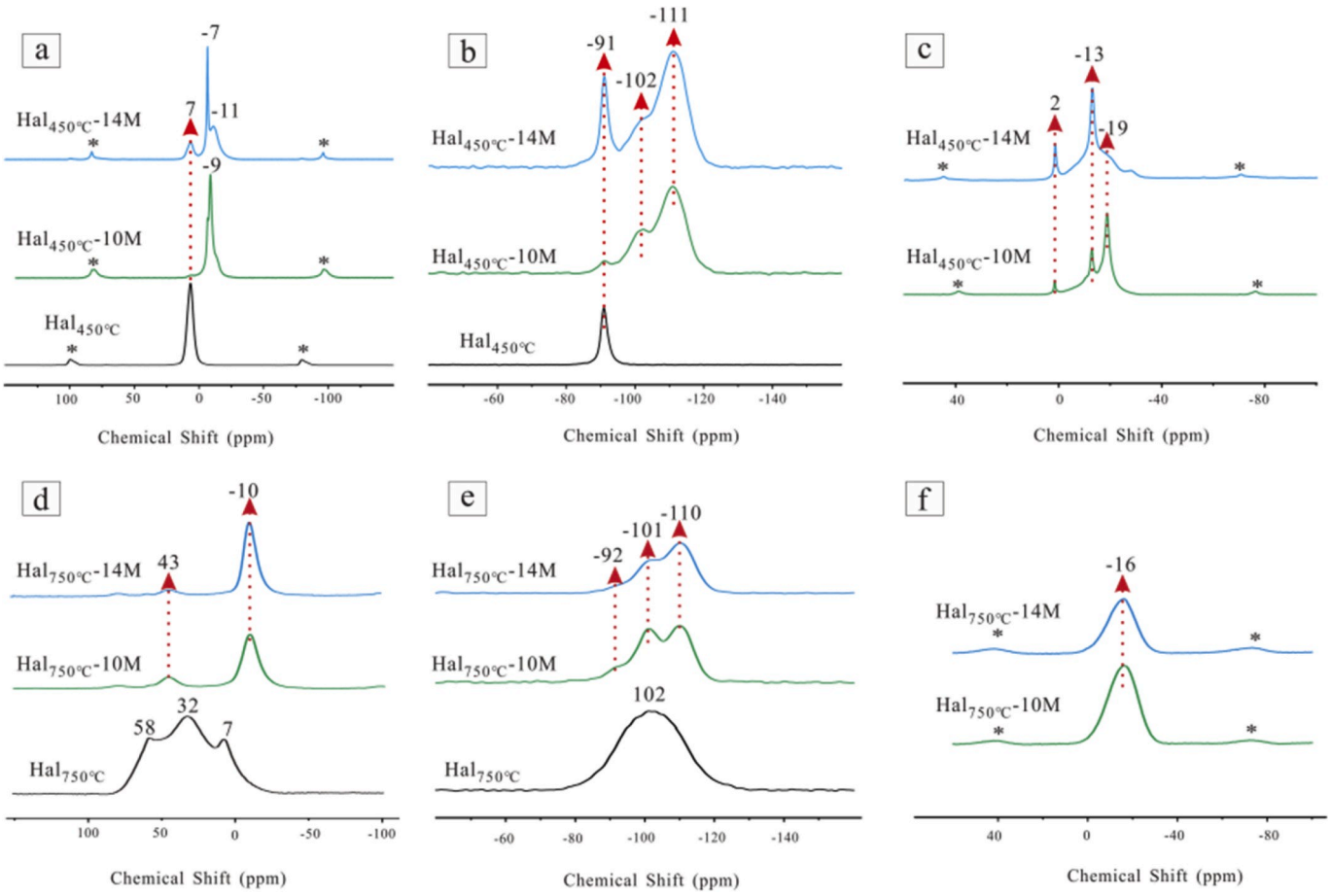

Fig. 6. (a, d) ^{27}Al MAS NMR spectra for Hal_T and its acid-activation products; (b, e) ^{29}Si MAS NMR spectra for Hal_T and its acid-activation products; and (c, f) ^{31}P MAS NMR spectra for acid-activated Hal_T.

(Fig. 6d), which were attributed to Al^{VI}, Al^{V}, and Al^{IV}, respectively, and suggested the existence of an amorphous phase [61]. In the ^{29}Si NMR spectrum of $Hal_{450°C}$ (Fig. 6b), the resonance located at −91 ppm was assigned to Q^3 from the layered structure in silicate [62]. The resonance became broader and shifted to a lower field (−102 ppm) when Hal was calcined at 750 °C, consistent with the formation of the disordered Q^3(3Si) environment [63].

It can be observed from the ^{27}Al NMR spectra that different phosphoric acid concentrations created different Al chemical environments in acid-activated $Hal_{450°C}$ (Fig. 6a). In the spectrum of $Hal_{450°C}$-10 M, the narrow resonance centered at −9 ppm was assigned to Al^{VI} [58], which can be attributed to metavariscite [64]. Additionally, the very weak resonance at approximately 7 ppm was ascribed to Al^{VI} from residual $Hal_{450°C}$. Significantly, when the concentration increased to 14 mol/L, the 7 ppm resonance increased in intensity, which was indicative of the presence of more unreacted $Hal_{450°C}$. Phosphoric acid tended to react with Al^{3+} that released from halloysite to form crystalline $AlPO_4$ at low concentration (10 mol/L), while react with the Al and Si to form amorphous geopolymer at high concentration (14 mol/L). Consequently, Different reaction processes resulted in the different dissolution behavior of $Hal_{450°C}$, causing more unreacted $Hal_{450°C}$ for 14 mol/L H_3PO_4. A broad resonance at −11 ppm was assigned to Al^{VI} of the geopolymer [65], while a narrow resonance at −7 ppm was attributed to Al^{VI} of the aluminophosphate [66,67].

In the ^{27}Al NMR spectra of acid-activated $Hal_{750°C}$ (Fig. 6d), two new resonances centered at about −10 and 43 ppm were present, but each had different content ratios. The former was attributed to Al^{VI} of acid-based geopolymer and the latter to Al^{IV} of $Al(PO)_4$ species [65]. Semi-quantitative estimation was used to show that the Al^{VI}/Al^{IV} ratio increased from 4.35 to 10.00 when the acid concentration increased from 10 mol/L to 14 mol/L, which indicated that increasing the concentration promoted the transformation from Al^{IV} into Al^{VI}, demonstrating that higher phosphoric acid concentration facilitated higher geopolymerization degree.

Table 2
SEM/EDX results of acid-activation geopolymers.

Sample	Elements (%, atomic ratio)			
	Si	Al	P	O
$Hal_{450°C}$-14M	5.3	7.3	12.7	74.7
$Hal_{750°C}$-6M	7.0	11.7	10.9	70.4
$Hal_{750°C}$-10M	8.0	9.4	10.7	71.9
$Hal_{750°C}$-14M	7.9	8.0	11.0	73.1

Three broad signals were observed in the ^{29}Si NMR spectra of acid-activated $Hal_{450°C}$. The resonance centered at −111 ppm was assigned to newly formed Q^4(0Al) of amorphous silica derived from dealumination of $Hal_{450°C}$. The resonances at −102 ppm and −91 ppm were attributed to Q^3-type $Si(OSi)_3(O^+AlH)$ sites and Q^3-type $Si(OSi)_3(OAl_2)$ sites, respectively [36]. Compared with $Hal_{450°C}$-10 M, $Hal_{450°C}$-14 M had higher intensity resonances at −91 ppm and −111 ppm, which indicated that greater amounts of unreacted $Hal_{450°C}$ and amorphous silica were present in this sample.

Three signals were also observed in the ^{29}Si NMR spectra of acid-activated $Hal_{750°C}$, at −92 ppm, −101 ppm, and −110 ppm (Fig. 6e). However, considering the results of XRD (Fig. 4) and SEM/EDX (Table 2), it was suggested that these resonances are actually related to Si^{IV}–O–P or Si^{IV}–O–Al from the acid-activated geopolymer [58]. It has

Table 3
TEM/EDX results of acid-activation products.

Sample	Elements (%, atomic ratio)			
	Si	Al	P	O
$Hal_{450°C}$-14M	3.2	9.8	15.5	71.5
$Hal_{750°C}$-10M	12.0	8.9	9.1	70.0
$Hal_{750°C}$-14M	10.1	9.2	13.1	67.6

been reported that the Si signal shifts to higher field as each tetrahedral [AlO_4] is connected to a tetrahedral [SiO_4], but to lower field as each tetrahedral [PO_4] is connected to a tetrahedral [SiO_4] [20,60,68]. Accordingly, it can be concluded that more P was incorporated into the geopolymeric matrix with increasing phosphoric acid concentration because the resonance at −110 ppm of $Hal_{750°C}$-10 M was more intense than that of $Hal_{750°C}$-14 M. However, the possible existence of unreacted $Hal_{750°C}$ and amorphous SiO_2 in the acid-based geopolymer cannot be ruled out [20]. Therefore, it was difficult to accurately discern the structural environment of Si in the acid-based geopolymer, which contained tetrahedral [AlO_4], [SiO_4], and [PO_4] and octahedral [AlO_6].

The ^{31}P NMR spectrum of $Hal_{450°C}$-10 M contained three sharp peaks (Fig. 6c). The first of these, located at 2 ppm, corresponded to the phosphorus environment of Q^0 generated by orthophosphate groups [69], while the second peak (−13 ppm) was attributable to the presence of polyphosphates [52]. The third peak (−19 ppm) was ascribed to Q^4(4Al) of metavariscite, wherein a [PO_4] unit was connected to four Al atoms by bridging O atoms [70]. The intensity of the peaks at −2 ppm and −13 ppm in the sample of $Hal_{450°C}$-14 M increased, due to the presence of more unreacted phosphoric acid. Meanwhile, the signal at −19 ppm broadened, which indicated the formation of amorphous phases.

In contrast, the ^{31}P NMR spectra of $Hal_{750°C}$-10 M and $Hal_{750°C}$-14 M (Fig. 6f) were similar to one another, containing only one broad peak at −16 ppm, which has been reported by others [24,58,65]. Some have attributed this peak to Q^1(2Al) of the aluminophosphate network, while others concluded that it should be attributed to a tetrahedral P [20,26]. Given the results of ^{29}Si NMR (Fig. 6e) and TEM/EDX (Table 3d), it is suggested that this peak is attributed to the Q^3(*x*Al, *y*Si) of the geopolymeric network [71], which is a typical substructure of acid-based geopolymers.

3.4. Morphology and microstructure of acid-activated Hal_T

3.4.1. SEM results

Fig. 7 shows the SEM images of the acid-activation products. $Hal_{450°C}$-10 M showed an inhomogeneous microstructure with macropores and voids (Fig. 7a), resulting in low compressive strength. Unreacted $Hal_{450°C}$ can also be identified in the matrix (marked by the pointing arrow). A similar microstructure can be observed for $Hal_{450°C}$-6M, as shown in Fig. S2a (Supplementary Information). However, $Hal_{450°C}$-14 M exhibited a different microstructure, with a texture that was homogeneous and highly continuous and devoid of microcracks (Fig. 7b).

$Hal_{750°C}$-14 M and $Hal_{750°C}$-10 M exhibited a much denser, more compact, and more homogeneous microstructure than $Hal_{750°C}$-6M (Figs. S2b and S2c). This densification of the microstructure of $Hal_{750°C}$-X indicated that increasing the acid concentration had improved the extent of geopolymerization, which was consistent with the corresponding increase in the compressive strength (Fig. 3). As shown in Fig. 7d, large quantities of nanosized tubes were visible in its acid-activation products even when the acid concentration was as high as 14 mol/L. Combining the SEM image of $Hal_{1000°C}$ (Fig. S1d) and TEM/EDX result of $Hal_{1000°C}$-14 M (Fig. 10a), these nanosized tubes should be unreacted $Hal_{1000°C}$.

EDX analyses were performed on the acid-based geopolymers ($Hal_{450°C}$-14 M, $Hal_{750°C}$-6M, $Hal_{750°C}$-10 M, and $Hal_{750°C}$-14 M). Thirty data points were collected at selected areas of each homogeneous geopolymeric matrix and the average values of the detected atom ratios are shown in Table 2. The results show that the geopolymeric matrix consisted of Si, Al, P, and O, which indicated the formation of a silico-alumino-phosphate (S-A-P) network in the geopolymeric matrix [26,52].

As shown in Table 2, the Si:Al:P ratios were different for each geopolymer. The Si/P ratio of $Hal_{450°C}$-14 M was much lower than that of

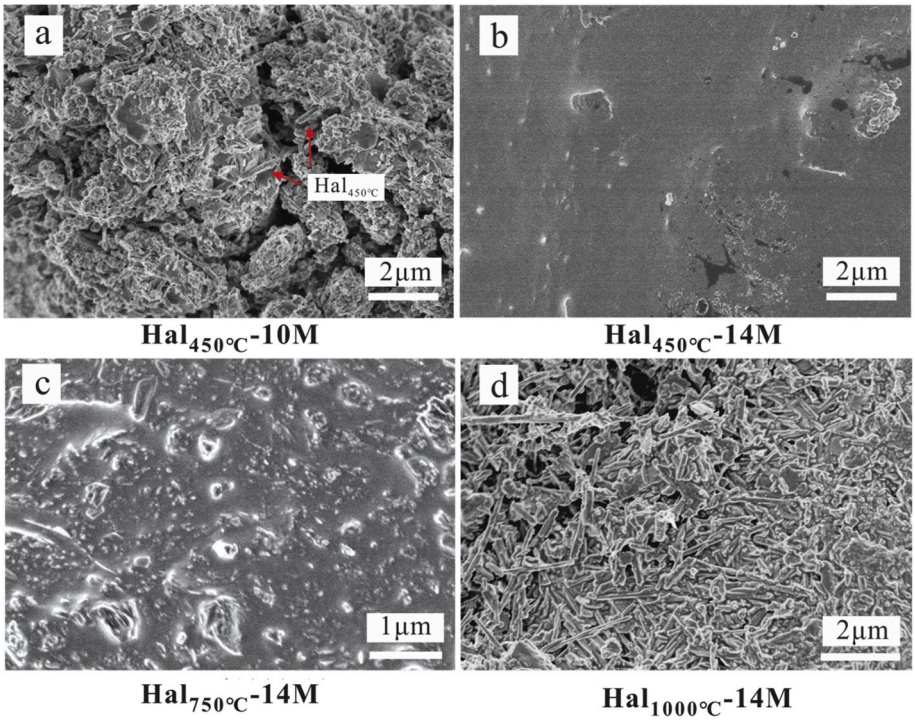

Fig. 7. SEM images of acid-activated Hal_T.

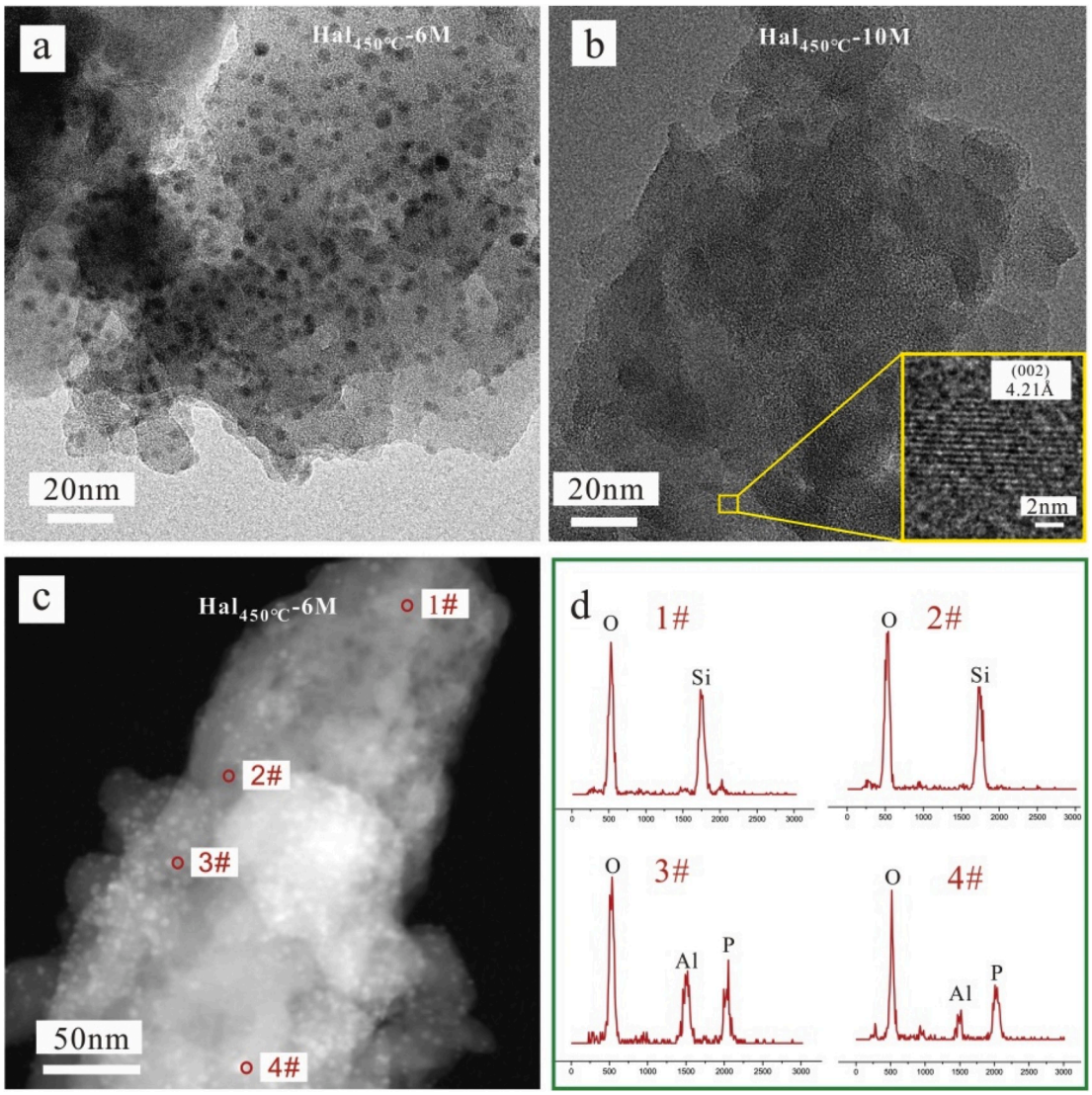

Fig. 8. TEM, high-resolution TEM (HRTEM), and high-angle annular dark-field scanning TEM (HAADF-STEM) images of acid-activated $Hal_{450°C}$. (a) TEM image of $Hal_{450°C}$-6M; (b) TEM images of $Hal_{450°C}$-10 M; (c) HAADF-STEM image of $Hal_{450°C}$-6M; (d) EDX spectrum of selected spots indicated by circles in (c).

the $Hal_{750°C}$-6M, $Hal_{750°C}$-10 M, and $Hal_{750°C}$-14 M, which indicated that less Si took part in the geopolymerization at lower precalcination temperatures. As the acid concentration was increased from 6 to 14 mol/L, the Si/P ratios of the products of acid-activated $Hal_{750°C}$ increased to approximately 0.73, although the Si/P ratios of their corresponding raw materials decreased due to the higher phosphoric acid concentration with constant liquid/solid ratio. This result indicated that more Si and P were incorporated into the geopolymeric networks with the increase of phosphoric acid concentration. Furthermore, although the concentration of Si leached from $Hal_{750°C}$ was much smaller than that of Al (Table 1), the Si/Al ratio of $Hal_{750°C}$-14 M was close to 1, as shown in Table 2, demonstrating that Si was incorporated into the geopolymer network in the form of amorphous SiO_2.

3.4.2. TEM results

Fig. 8 shows TEM images of phosphoric acid-activated $Hal_{450°C}$. It can be observed that many nanoparticles are distributed in the $Hal_{450°C}$-6M matrix, whose diameter is approximately 3 nm (Fig. 8a). According to the EDS results, these nanoparticles were mainly composed of Al, O, and P atoms, while the matrix mainly consisted of Si and O atoms (Fig. 8c and d). This reflected that Al released from $Hal_{450°C}$ reacted with phosphoric acid locally to form $AlPO_4$-compounds. In the meantime, the dealumination of $Hal_{450°C}$ led to the formation of amorphous silica [42,58]. For $Hal_{450°C}$-10 M, there were lattice fringes with an interplanar distance of 4.21 Å (Fig. 8b). This value corresponded well with the *d*-spacing value of the (002) for metavariscite. This was also evidenced by elemental mapping results of $Hal_{450°C}$-10 M (Fig. S3), where the atom ratio of P:Al:Si was 7.0:6.7:18.1. P was positively correlated with Al, but showed a weak correlation with Si.

TEM images and EDX mapping of the halloysite-based geopolymers are presented in Fig. 9 and the EDX results of the selected areas are displayed in Table 3. $Hal_{450°C}$-14 M exhibited two separated phases, with one enriched with Si and the other with Al and P (Fig. 9a). By comparing the XRD (Fig. 4) and NMR results (Fig. 6b), the Si-rich phase can be identified as amorphous silica while the Al–O–P-rich phase was the geopolymer. Therefore, the geopolymer derived from $Hal_{450°C}$ was mainly composed of Al–O–P units, in which the P content was higher than the Al content (Table 3). Significantly, a small amount of Si was also distributed in the geopolymer matrix, which indicated that the network can be characterized as Si–O–P–O–Al. In addition, the geopolymeric matrix was evidently less porous and more compact than amorphous silica.

It can be observed from Fig. 9b and c that Si, Al, and P were evenly distributed throughout the geopolymeric matrix of $Hal_{750°C}$ acid-

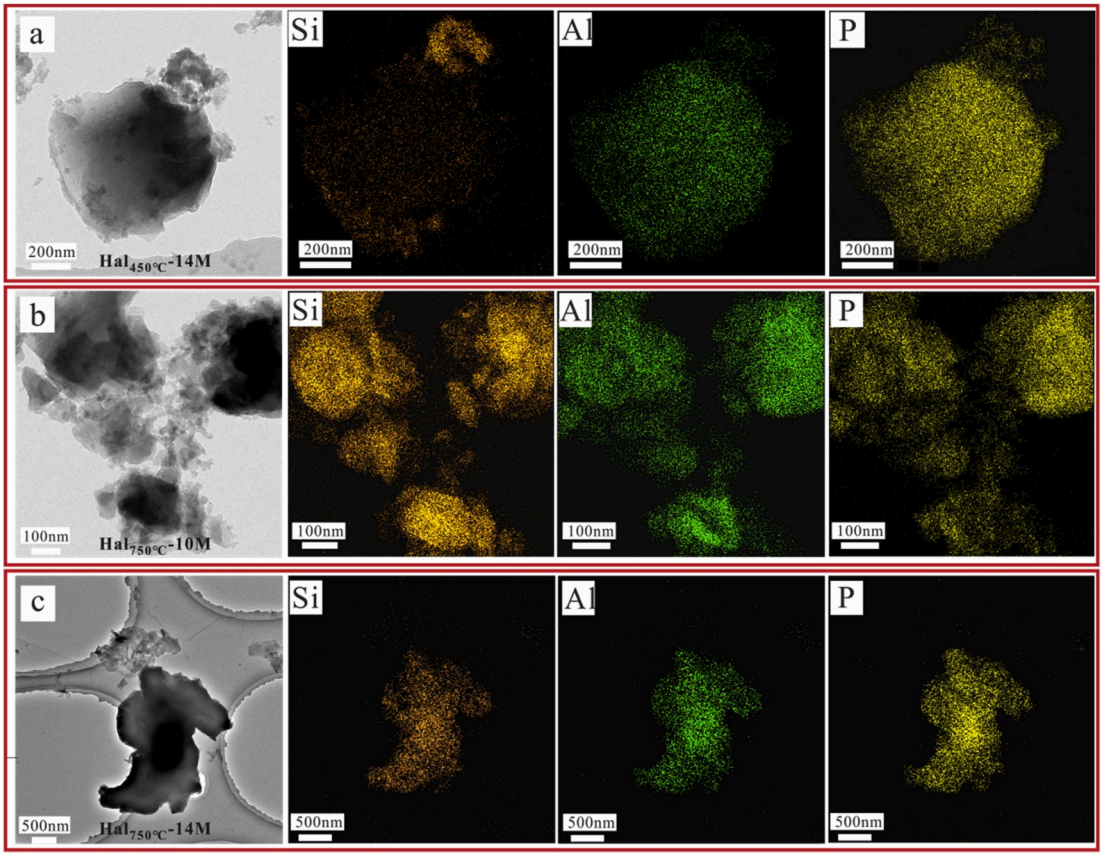

Fig. 9. TEM images with elemental mapping of acid-activation geopolymers: (a) $Hal_{450°C}$-14 M; (b) $Hal_{750°C}$-10 M; (c) $Hal_{750°C}$-14 M.

activated by 10 mol/L and 14 mol/L phosphoric acid. Additionally, $Hal_{750°C}$-10 M and $Hal_{750°C}$-14 M contained much more Si than $Hal_{450°C}$-14 M (Table 3), which was consistent with the SEM/EDX analysis and demonstrated that more Si was incorporated into the geopolymeric matrix in the products of acid-activated $Hal_{750°C}$. Therefore, unlike $Hal_{450°C}$-14 M, the geopolymers derived from $Hal_{750°C}$ were mainly composed of Si–O–Al–O–P units.

As presented in Fig. 10, two different products appeared in $Hal_{1000°C}$-6M. Nanosized tubes, which mainly consisted of Si, Al, and O, were abundant in acid-activated $Hal_{1000°C}$ (Fig. 10a and b), which corresponded to unreacted $Hal_{1000°C}$. However, a small number of products with a porous microstructure consisting of Si, Al, P, and O (Fig. 10c and d) were also observed. Si, P, and Al were evenly distributed in the matrix (Fig. S4), which is most likely to be the result of geopolymerization. These results indicated that $Hal_{1000°C}$ was mostly unreactive with phosphoric acid, aside from a small amount of residual species (amorphous Al_2O_3 and amorphous SiO_2) possibly reacting with phosphoric acid to form a Si–O–P–O–Al network. However, the resulting geopolymeric content was too low to impart any compressive strength to the material as a whole.

4. Discussion

Nanosized tubular halloysite not only has high specific surface area but also provides a large number of reaction sites, making it a suitable geopolymer precursor [40]. It has a similar chemical composition to plate-like kaolinite, but the calcination-induced changes in the structure and surface activity of halloysite are quite different from those of kaolinite. Therefore, halloysite shows both similarities and differences with respect to other precursors (especially kaolinite) during acid-activation [23,26,65].

The abovementioned findings indicated that similar to kaolinite [26], halloysite subject to precalcination at an appropriate temperature shows greatly improved reactivity of acid-based geopolymerization. Dehydroxylation of halloysite was previously reported to occur at ~500°C-900 °C, resulting in the loss of long-range order and the disconnection of silica and alumina into separate amorphous phases [43]. Likewise, geopolymers derived from acid-activation of halloysite are also amorphous, which is analogous to the behavior of acid-activated kaolinite-based geopolymers [58,65].

However, the findings of this work also indicated that the geopolymerization mechanism of acid-activated halloysite, including reaction process and geopolymeric network composition, differs substantially from that of acid-activated kaolinite. In this study, Si was not leached out of the halloysite, and indeed its dissolution was not necessary for geopolymer formation during acid-based geopolymerization. Instead, Si was incorporated directly into the geopolymer network in the form of amorphous SiO_2, which contained silanols that reacted with phosphoric acid through the polycondensation between Si–OH and P–OH to form P–O–Si networks [65,71]. Meanwhile, PO_4^{3-} readily reacted with Al^{3+} to form Al–O–P bonds due to the strong affinity between P and Al [65,71,72]. For example, during geopolymerization of $Hal_{750°C}$, phosphoric acid not only reacted with amorphous Al_2O_3 to form P–O–Al networks, but reacted with amorphous SiO_2 to form P–O–Si networks [71]. Consequently, a geopolymer with Si–O–P–O–Al networks was formed, which was evidenced by the distribution of Si, Al, and P atoms (Fig. 9b and c). Moreover, the densification of the microstructures and strength gains of the geopolymers activated with different concentrations of phosphoric acid demonstrated that the geopolymerization degree had been enhanced by increasing concentrations of phosphoric acid, which was due to the inclusion of more Si and P in the geopolymeric network. This contrasts with some previous studies on acid-activation of kaolinite other than halloysite, which reported that geopolymeric networks were formed

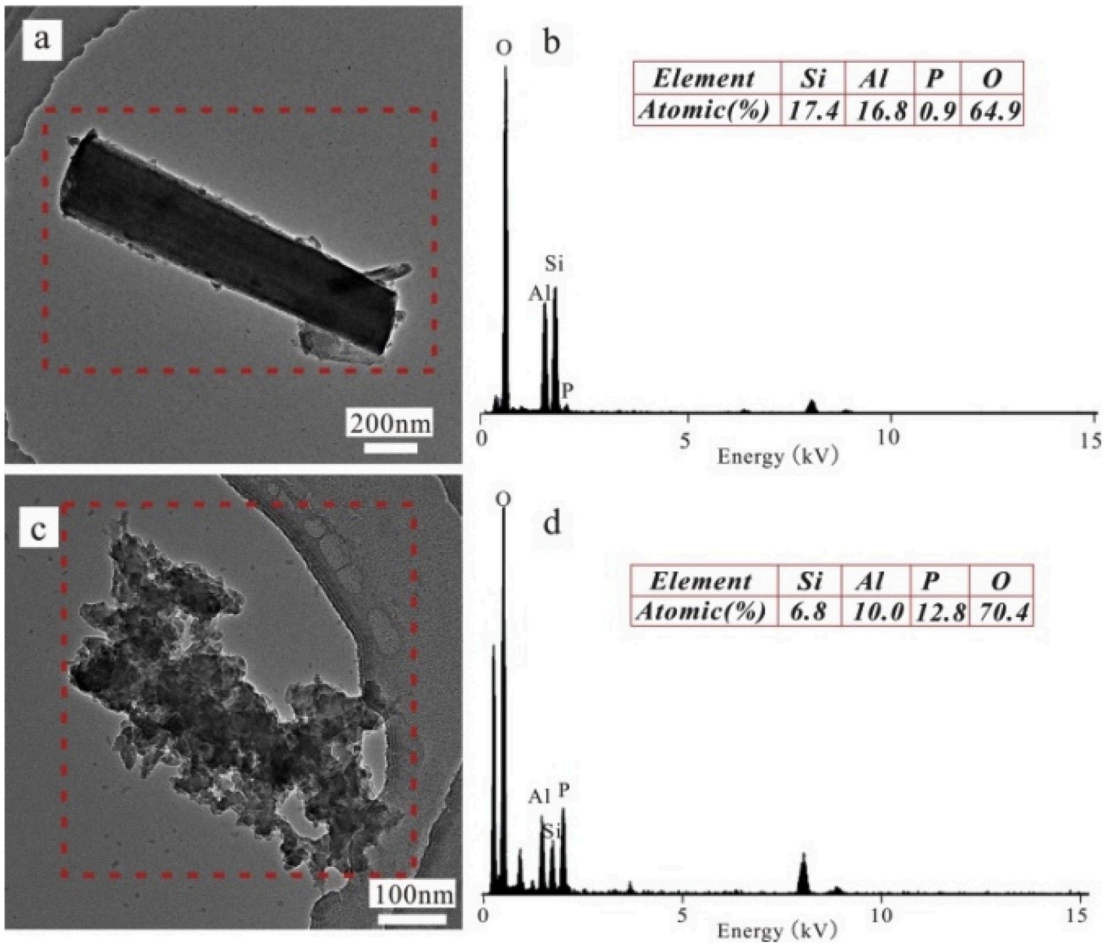

Fig. 10. (a), (c)TEM images of $Hal_{1000°C}$-6M; (b) EDX spectrum of a selected area indicated by a rectangle in (a); (d) EDX spectrum of a selected area indicated by a rectangle in (c).

through the reaction between low-polymeric [PO_4] tetrahedral units and active Al–O in metakaolinite [73] or through the polycondensation of free silicate, aluminate, and phosphate units [52,74] for acid-activation of kaolinite. Moreover, previous studied have proposed that the acid-activation of kaolinite produced a geopolymer consisting of a Si–O–P network and $AlPO_4$ crystals [23,25,28], which is also different from the acid-activation of halloysite. These contrasting reactivities can be attributed to the different structures and surface reactivity of halloysite and kaolinite. Compared with kaolinite, nanosized tubular halloysite has higher reactivity and more sites exposed to the acid activator, and can form hydroxyl groups at the outer surface after precalcination [46,75]. Therefore, phosphoric acid will more readily combine with Al and Si during geopolymerization, which thus induces the formation of Si–O–P–O–Al networks. Collectively, these results indicated that halloysite has excellent geopolymerization reactivity in acid-activation systems, and can produce long chains of poly (silico-alumino-phosphate). Therefore, acid-activation of halloysite is likely to afford materials with properties superior to those derived from acid-activated kaolinite.

Furthermore, of particular interest is that the reaction process of acid-activation of halloysite calcined at low temperature (450 °C) can be altered by changing the phosphoric acid concentration. For example, the acid-activation process of $Hal_{450°C}$ appeared to start with the dissolution of halloysite, leading to the release of Al^{3+} and the formation of amorphous SiO_2 [36,42], both of which further reacted with phosphoric acid. At low phosphoric acid concentrations (≤10 mol/L), metavariscite crystals were formed; however, at a high concentration (14 mol/L), a geopolymer with Si–O–P–O–Al networks was formed. This difference is due to the behavior of the abundant silanols that were formed for $Hal_{450°C}$, as a consequence of the high specific surface area, after the release of Al^{3+}. Therefore, when the phosphoric acid concentration was sufficiently high, large numbers of polyphosphate species (e.g., acid dimers $H_5P_2O_8^-$ and $H_6P_2O_8$) [64,69] appeared to induce the formation of Al–O–P and Si–O–P networks. However, similar observations have not been reported for acid-activated kaolinite.

As discussed above, the difference in structure between halloysite and kaolinite is one of the most important factors leading to the different acid-based geopolymerization behaviors. Nanosized tubular halloysite, as a highly active geopolymer precursor, tends to form a geopolymeric network during acid-activation, leading to improved geopolymeric performance. Therefore, halloysite is a promising precursor for acid-based geopolymer synthesis and warrants further study.

5. Conclusions

Halloysite is a promising geopolymer precursor because of its nanosized tubular structure. Here we have presented some initial results from our investigation of the activation of halloysite with phosphoric acid. A combination of spectroscopic and microscopic techniques was used to investigate the effects of precalcination temperature and phosphoric acid concentration on the microstructure and mechanical performance of the resultant halloysite-based geopolymer.

Halloysite calcined at 450 °C had low reactivity due to its high crystallinity and chemical stability. Acid-activation of this calcined halloysite with low concentrations of phosphoric acid (≤10 mol/L) produced metavariscite crystals with a porous structure. When the

concentration was increased to 14 mol/L, large numbers of polyphosphates in phosphoric acid solution reacted with dissolved Al^{3+} to form a compact geopolymer, which mainly consisted of Al–O–P networks. Meanwhile, the phosphoric acid also reacted with amorphous SiO_2 via reaction between Si–OH and P–OH to form Si–O–P networks, but to a lesser extent. Calcination at 750 °C improved the reactivity of halloysite due to dehydroxylation. Consequently, during acid-activation of $Hal_{750°C}$, phosphoric acid reacted with both amorphous Al_2O_3 and amorphous SiO_2 to form a geopolymer with Si–O–P–O–Al network. The extent of geopolymerization was enhanced by increased phosphoric acid concentration due to incorporation of more Si and P into the geopolymeric network, which led to the formation of a denser structure with increased compressive strength. However, halloysite calcined at 1000 °C was largely unreactive with phosphoric acid, as it contained γ-Al_2O_3 and had a lower Si–OH content.

This study has provided important insights into the reaction mechanism of acid-activated halloysite, which will play a fundamental role in further understanding and utilizing this mineral as a precursor for preparation of acid-based geopolymers. The microstructure and mechanical performance of acid-activated halloysite have been shown to be strongly dependent on the halloysite structure and the concentration of phosphoric acid used in its preparation. In addition, modifying the way in which Si and P are incorporated into the acid-based geopolymer matrix was found to be an effective way to generate high-performance halloysite-based geopolymer materials.

Declaration of competing interest

The authors declare that there is no conflict of interest.

Acknowledgements

Financial supports from the National Natural Science Foundation of China (Grant Nos. 41972045 and 41672042), National Special Support for High-Level Personnel and Youth Innovation Promotion Association CAS for the excellent members (2016-81-01) and Science and Technology Planning Project of Guangdong Province, China (2017B020237003) are gratefully acknowledged. This is a contribution (No.IS-2843) from GIGCAS.

Appendix A. Supplementary data

Supplementary data to this article can be found online at https://doi.org/10.1016/j.cemconcomp.2020.103601.

References

[1] J. Davidovits, Geopolymers: inorganic polymeric new materials, J. Therm. Anal. Calorim. 37 (8) (1991) 1633–1656.
[2] P. Duxson, A. Fernández-Jiménez, J.L. Provis, G.C. Lukey, A. Palomo, J.S.J. V. Deventer, Geopolymer technology: the current state of the art, J. Mater. Sci. 42 (9) (2007) 2917–2933.
[3] S.J.K. Melele, H.K. Tchakouté, C. Banenzoué, E. Kamseu, C.H. Rüscher, F. Andreola, C. Leonelli, Investigation of the relationship between the condensed structure and the chemically bonded water content in the poly(sialate-siloxo) network, Appl. Clay Sci. 156 (2018) 77–86.
[4] A. Font, M.V. Borrachero, L. Soriano, J. Monzo, A. Mellado, J. Paya, New eco-cellular concretes: sustainable and energy-efficient materials, Green Chem. 20 (20) (2018) 4684–4694.
[5] R.Y. Nkwaju, J.N.Y. Djobo, J.N.F. Nouping, P.W.M. Huisken, J.G.N. Deutou, L. Courard, Iron-rich laterite-bagasse fibers based geopolymer composite: mechanical, durability and insulating properties, Appl. Clay Sci. 183 (2019), 105333.
[6] C. Zanotti, P.H.R. Borges, A. Bhutta, N. Banthia, Bond strength between concrete substrate and metakaolin geopolymer repair mortar: effect of curing regime and PVA fiber reinforcement, Cement Concr. Compos. 80 (2017) 307–316.
[7] B.C. McLellan, R.P. Williams, J. Lay, A. van Riessen, G.D. Corder, Costs and carbon emissions for geopolymer pastes in comparison to ordinary portland cement, J. Clean. Prod. 19 (9) (2011) 1080–1090.
[8] C. Shi, A.F. Jiménez, A. Palomo, New cements for the 21st century: the pursuit of an alternative to Portland cement, Cem. Concr. Res. Cem. Concr. Res. 41 (7) (2011) 750–763.
[9] M. Farooq, A. Bhutta, N. Banthia, Tensile performance of eco-friendly ductile geopolymer composites (EDGC) incorporating different micro-fibers, Cement Concr. Compos. 103 (2019) 183–192.
[10] B. Walkley, X. Ke, O.H. Hussein, S.A. Bernal, J.L. Provis, Incorporation of strontium and calcium in geopolymer gels, J. Hazard Mater. 382 (2020), 121015.
[11] M.X. Xu, Y. He, Z.H. Liu, Z.F. Tong, X.M. Cui, Preparation of geopolymer inorganic membrane and purification of pulp-papermaking green liquor, Appl. Clay Sci. 168 (2019) 269–275.
[12] F. Colangelo, G. Roviello, L. Ricciotti, V. Ferrándiz-Mas, F. Messina, C. Ferone, O. Tarallo, R. Cioffi, C.R. Cheeseman, Mechanical and thermal properties of lightweight geopolymer composites, Cement Concr. Compos. 86 (2018) 266–272.
[13] N. Roghanian, N. Banthia, Development of a sustainable coating and repair material to prevent bio-corrosion in concrete sewer and waste-water pipes, Cement Concr. Compos. 100 (2019) 99–107.
[14] E.N. Kani, A. Allahverdi, J.L. Provis, Efflorescence control in geopolymer binders based on natural pozzolan, Cement Concr. Compos. 34 (1) (2012) 25–33.
[15] Y. Alrefaei, J.-G. Dai, Silico-aluminophosphate and alkali-aluminosilicate geopolymers: a comparative review, Front. Mater. 6 (2019) 106.
[16] B. Zhang, H. Guo, P. Yuan, Y. Li, Q. Wang, L. Deng, D. Liu, Geopolymerization of halloysite via alkali-activation: dependence of microstructures on precalcination, Appl. Clay Sci. 185 (2020), 105375.
[17] Z.M. Li, S.Z. Zhang, Y.B. Zuo, W. Chen, G. Ye, Chemical deformation of metakaolin based geopolymer, Cement Concr. Res. 120 (2019) 108–118.
[18] M. Zribi, B. Samet, S. Baklouti, Mechanical, microstructural and structural investigation of phosphate-based geopolymers with respect to P/Al molar ratio, J. Solid State Chem. 281 (2020), 12025.
[19] X.M. Cui, L.P. Liu, H. Yan, J.Y. Chen, Z. Ji, A novel aluminosilicate geopolymer material with low dielectric loss, Mater. Chem. Phys. 130 (1) (2011) 1–4.
[20] D.S. Perera, J.V. Hanna, J. Davis, M.G. Blackford, B.A. Latella, Y. Sasaki, E. R. Vance, Relative strengths of phosphoric acid-reacted and alkali-reacted metakaolin materials, J. Mater. Sci. 43 (19) (2008) 6562–6566.
[21] L. Liu, X. Cui, S. Qiu, J. Yu, Z. Lin, Preparation of phosphoric acid-based porous geopolymers, Appl. Clay Sci. 50 (4) (2010) 600–603.
[22] H. Douiri, S. Louati, S. Baklouti, M. Arous, Z. Fakhfakh, Structural, thermal and dielectric properties of phosphoric acid-based geopolymers with different amounts of H_3PO_4, Mater. Lett. 116 (2014) 9–12.
[23] S. Louati, S. Baklouti, B. Samet, Acid based geopolymerization kinetics: effect of clay particle size, Appl. Clay Sci. 132 (2016) 571–578.
[24] M. Zribi, B. Samet, S. Baklouti, Effect of curing temperature on the synthesis, structure and mechanical properties of phosphate-based geopolymers, J. Non-Cryst. Solids 511 (2019) 62–67.
[25] H.K. Tchakoute, C.H. Ruscher, E. Kamseu, F. Andreola, C. Leonelli, Influence of the molar concentration of phosphoric acid solution on the properties of metakaolin-phosphate-based geopolymer cements, Appl. Clay Sci. 147 (2017) 184–194.
[26] H. Yan, L. Liu, L. He, X. Cui, Characterization of chemosynthetic H_3PO_4–Al_2O_3–$2SiO_2$ geopolymers, Ceram. Int. 42 (9) (2016) 10908–10912.
[27] M.L. Gualtieri, M. Romagnoli, S. Pollastri, A.F. Gualtieri, Inorganic polymers from laterite using activation with phosphoric acid and alkaline sodium silicate solution: mechanical and microstructural properties, Cement Concr. Res. 67 (2015) 259–270.
[28] H. Douiri, S. Louati, S. Baklouti, M. Arous, Z. Fakhfakh, Structural and dielectric comparative studies of geopolymers prepared with metakaolin and Tunisian natural clay, Appl. Clay Sci. 139 (2017) 40–44.
[29] A. Elimbi, H.K. Tchakoute, D. Njopwouo, Effects of calcination temperature of kaolinite clays on the properties of geopolymer cements, Construct. Build. Mater. 25 (6) (2011) 2805–2812.
[30] J. Li, X. Zuo, X. Zhao, J. Ouyang, H. Yang, Insight into the effect of crystallographic structure on thermal conductivity of kaolinite nanoclay, Appl. Clay Sci. 173 (2019) 12–18.
[31] L. Deng, P. Yuan, D. Liu, F. Annabi-Bergaya, J. Zhou, F. Chen, Z. Liu, Effects of microstructure of clay minerals, montmorillonite, kaolinite and halloysite, on their benzene adsorption behaviors, Appl. Clay Sci. 143 (2017) 184–191.
[32] E. Joussein, Chapter 2 - geology and mineralogy of nanosized tubular halloysite, in: P. Yuan, A. Thill, F. Bergaya (Eds.), Developments in Clay Science, Elsevier, 2016, pp. 12–48.
[33] E. Joussein, S.G. Petit, J. Churchman, B.K.G. Theng, D. Righi, B. Delvaux, Halloysite clay minerals - a review, Clay Miner. 40 (4) (2005) 383–426.
[34] P. Yuan, P.D. Southon, Z.W. Liu, M.E.R. Green, J.M. Hook, S.J. Antill, C.J. Kepert, Functionalization of halloysite clay nanotubes by grafting with gamma-aminopropyltriethoxysilane, J. Phys. Chem. C 112 (40) (2008) 15742–15751.
[35] L. Deng, P. Yuan, D. Liu, P. Du, J. Zhou, Y. Wei, Y. Song, Y. Liu, Effects of calcination and acid treatment on improving benzene adsorption performance of halloysite, Appl. Clay Sci. 181 (2019), 105240.
[36] A. Elshad, J. Anupam, W. Wenbo, Z. Yafei, L. Yuri, Enlargement of halloysite clay nanotube lumen by selective etching of aluminum oxide, ACS Nano 6 (8) (2012) 7216–7226.
[37] P. Yuan, D. Tan, F. Annabi-Bergaya, Properties and applications of halloysite nanotubes: recent research advances and future prospects, Appl. Clay Sci. 112 (2015) 75–93.
[38] V. Zivica, M.T. Palou, T.I.Ľ. Bágeľ, High strength metahalloysite based geopolymer, Compos. B Eng. 57 (2014) 155–165.
[39] H.K. Tchakouté, S.J.K. Melele, A.T. Djamen, C.R. Kaze, E. Kamseu, C.N.P. Nanseu, C. Leonelli, C.H. Rüscher, Microstructural and mechanical properties of poly (sialate-siloxo) networks obtained using metakaolins from kaolin and halloysite as aluminosilicate sources: a comparative study, Appl. Clay Sci. 186 (2020), 105448.

[40] Z. Zhang, H. Wang, X. Yao, Y. Zhu, Effects of halloysite in kaolin on the formation and properties of geopolymers, Cement Concr. Compos. 34 (5) (2012) 709–715.
[41] C.R. Kaze, H.K. Tchakoute, T.T. Mbakop, J.R. Mache, E. Kamseu, U.C. Melo, C. Leonelli, H. Rahier, Synthesis and properties of inorganic polymers (geopolymers) derived from Cameroon-meta-halloysite, Ceram. Int. 44 (15) (2018) 18499–18508.
[42] R.D. White, D.V. Bavykin, F.C. Walsh, The stability of halloysite nanotubes in acidic and alkaline aqueous suspensions, Nanotechnology 23 (6) (2012), 065705.
[43] P. Yuan, Chapter 7 - thermal-treatment-induced deformations and modifications of halloysite, in: P. Yuan, A. Thill, F. Bergaya (Eds.), Developments in Clay Science, Elsevier, 2016, pp. 137–166.
[44] R.L. Frost, A.M. Vassallo, The dehydroxylation of the kaolinite clay minerals using infrared emission spectroscopy, Clay Clay Miner. 44 (5) (1996) 635–651.
[45] M.E. Smith, G. Neal, M.B. Trigg, J. Drennan, Structural characterization of the thermal transformation of halloysite by solid state NMR, Appl. Magn. Reson. 4 (1993) 157–170.
[46] P. Yuan, D. Tan, F. Aannabi-Bergaya, W. Yan, M. Fan, D. Liu, H. He, Changes in structure, morphology, porosity, and surface activity of mesoporous halloysite nanotubes under heating, Clay Clay Miner. 60 (6) (2012) 561–573.
[47] D. Liu, P. Yuan, D. Tan, H. Liu, T. Wang, M. Fan, J. Zhu, H. He, Facile preparation of hierarchically porous carbon using diatomite as both template and catalyst and methylene blue adsorption of carbon products, J. Colloid Interface Sci. 388 (1) (2012) 176–184.
[48] T.H. Wang, T.Y. Liu, D.C. Wu, M.H. Li, J.R. Chen, S.P. Teng, Performance of phosphoric acid activated montmorillonite as buffer materials for radioactive waste repository, J. Hazard Mater. 173 (1) (2010) 335–342.
[49] C. Pesquera, F. Gonzalez, I. Benito, C. Blanco, S. Mendioroz, J. Pajares, Passivation of a montmorillonite by the silica created in acid activation, J. Mater. Chem. 2 (9) (1992) 907.
[50] N.A. Milne, T. O'Reilly, P. Sanciolo, E. Ostarcevic, M. Beighton, K. Taylor, M. Mullett, A.J. Tarquin, S.R. Gray, Chemistry of silica scale mitigation for RO desalination with particular reference to remote operations, Water Res. 65 (2014) 107–133.
[51] M. Lizcano, A. Gonzalez, S. Basu, K. Lozano, M. Radovic, D. Viehland, Effects of water content and chemical composition on structural properties of alkaline activated metakaolin-based geopolymers, J. Am. Ceram. Soc. 95 (7) (2012) 2169–2177.
[52] Y.S. Wang, J.L. Provis, J.G. Dai, Role of soluble aluminum species in the activating solution for synthesis of silico-aluminophosphate geopolymers, Cement Concr. Compos. 93 (2018) 186–195.
[53] J. Madejová, P. Komadel, Baseline studies of the clay minerals society source clays, Clay Clay Miner. 49 (5) (2001) 372–373.
[54] M. Rossi, R. Rizzi, A. Vergara, F. Capitelli, R.M. Ghiara, Compositional variation of turquoise group minerals from historical collection of the Real Museo Mineralogico of the University of Naples, Mineral. Mag. 81 (6) (2017) 1405–1429.
[55] W. Jastrzebski, M. Sitarz, M. Rokita, K. Bulat, Infrared spectroscopy of different phosphates structures, Spectrosc. Acta Pt. A Mol. Biomol. Spectr. 79 (4) (2011) 722–727.
[56] R.L. Frost, W.N. Martens, P.A. Williams, Raman and infrared spectroscopic study of the vivianite-group phosphates vivianite, baricite and bobierrite, Mineral. Mag. 66 (6) (2002) 1063–1073.
[57] M. Zaarour, O. Perez, P. Boullay, J. Martens, B. Mihailova, K. Karaghiosoff, L. Palatinus, S. Mintova, Synthesis of new cobalt aluminophosphate framework by opening a cobalt methylphosphonate layered material, CrystEngComm 19 (34) (2017) 5100–5105.
[58] V. Mathivet, J. Jouin, A. Gharzouni, I. Sobrados, H. Celerier, S. Rossignol, M. Parlier, Acid-based geopolymers: understanding of the structural evolutions during consolidation and after thermal treatments, J. Non-Cryst. Solids 512 (2019) 90–97.
[59] G. Bekiaris, C. Peltre, L.S. Jensen, S. Bruun, Using FTIR-photoacoustic spectroscopy for phosphorus speciation analysis of biochars, Spectrosc. Acta Pt. A Mol. Biomol. Spectr. 168 (2016) 29–36.
[60] A. Styskalik, D. Skoda, Z. Moravec, J.G. Abbott, C.E. Barnes, J. Pinkas, Synthesis of homogeneous silicophosphate xerogels by non-hydrolytic condensation reactions, Microporous Mesoporous Mater. 197 (2014) 204–212.
[61] W. Qian, R. Feng, S. Song, Reexamining calcination of kaolinite for the synthesis of metakaolin geopolymers - roles of dehydroxylation and recrystallization, J. Non-Cryst. Solids 460 (2017) 74–80.
[62] K. Yan, Y. Guo, L. Fang, L. Cui, F. Cheng, T. Li, Decomposition and phase transformation mechanism of kaolinite calcined with sodium carbonate, Appl. Clay Sci. 147 (2017) 90–96.
[63] T. Wang, X. Lu, Y. Yan, Synthesis, characterization and crystallization mechanism of SAPOs from natural kaolinite, Microporous Mesoporous Mater. 136 (1) (2010) 138–147.
[64] M. Cherif, A. Mgaidi, N. Ammar, G. Vallée, W. Fürst, A new investigation of aqueous orthophosphoric acid speciation using Raman spectroscopy, J. Solut. Chem. 29 (3) (2000) 255–269.
[65] H. Celerier, J. Jouin, A. Gharzouni, V. Mathivet, I. Sobrados, N. Tessier-Doyen, S. Rossignol, Relation between working properties and structural properties from ^{27}Al, ^{29}Si and ^{31}P NMR and XRD of acid-based geopolymers from 25 to 1000°C, Mater. Chem. Phys. 228 (2019) 293–302.
[66] C.P. Odriozola, A new approach to determine the geological provenance of variscite artifacts using the P/Al atomic ratios, Archaeol Anthrop. Sci. 7 (3) (2015) 329–350.
[67] S.J. Duffy, G.W.V. Loon, Investigations of aluminum hydroxyphosphates and activated sludge by ^{27}Al and ^{31}P MAS NMR, Can. J. Chem. 73 (73) (1995) 1645–1659.
[68] M.A. Wilson, S.A. McCarthy, P.M. Fredericks, Structure of poorly-ordered aluminosilicates, Clay Miner. 21 (5) (1986) 879–897.
[69] A. Samadi-Maybodi, S.K.H. Nejad-Darzi, H. Bijanzadeh, ^{31}P and ^{27}Al NMR studies of aqueous (2-hydroxyethyl) trimethylammonium solutions containing aluminum and phosphorus, Spectrosc. Acta Pt. A Mol. Biomol. Spectr. 72 (2) (2009) 382–389.
[70] C.S. Blackwell, R.L. Patton, Al-27 and P-31 nuclear magnetic-resonance studies of aluminophosphate molecular-sieves, J. Phys. Chem. 88 (25) (1984) 6135–6139.
[71] G.D. Cody, B. Mysen, G. Sághi-Szabó, J.A. Tossell, Silicate-phosphate interactions in silicate glasses and melts: I. A multinuclear (^{27}Al, ^{29}Si, ^{31}P) MAS NMR and ab initio chemical shielding (^{31}P) study of phosphorous speciation in silicate glasses, Geochem. Cosmochim. Acta 65 (14) (2001) 2395–2411.
[72] G. Tricot, B. Doumert, B. Revel, M. Bria, J. Trebosc, H. Vezin, Non-homogeneous distribution of Al^{3+} in doped phosphate glasses revealed by ^{27}Al/^{31}P solid state NMR, Solid State Nucl. Magn. Reson. 84 (2017) 137–142.
[73] D. Cao, D. Su, B. Lu, Y. Yang, Synthesis and structure characterization of geopolymeric material based on metakaolinite and phosphoric acid, J. Chin. Silic. Soc. 33 (11) (2005) 1385–1389.
[74] C.Y. Bai, A. Conte, P. Colombo, Open-cell phosphate-based geopolymer foams by frothing, Mater. Lett. 188 (2017) 379–382.
[75] B.A. Morrow, A.J. Mcfarlan, Surface vibrational modes of silanol groups on silica, J. Phys. Chem. 96 (3) (1992) 1395–1400.